Micro-inverter for Integrated Grid-tie PV Module Using Resonant Controller

Jonas Rafael Gazoli, Marcelo Gradella Villalva, Thais G. Siqueira, Ernesto Ruppert

***Abstract* – Two-stage isolated converters for photovoltaic (PV) applications commonly employ a high-frequency transformer on the DC-DC side, submitting the DC-AC inverter switches to high voltages and forcing the use of IGBTs instead of low-voltage and low-loss MOSFETs. This paper shows the modeling, control and simulation of a single-phase full-bridge inverter with high-frequency transformer (HFT) that can be used as part of a two-stage converter with transformerless DC-DC side or as a single-stage converter (simple DC-AC inverter) for grid-connected PV applications. The inverter is modeled in order to obtain a small-signal transfer function used to design the P+Resonant current control regulator. A high-frequency step-up transformer results in reduced voltage switches and better efficiency compared with converters in which the transformer is used on the DC-DC side. Simulations and experimental results with a 200 W prototype are shown.**

***Keywords* – AC-DC power converters, distributed power generation, modeling, photovoltaic systems, power transformers, pulse width modulation inverters.**

I. INTRODUCTION

Renewable energy, especially solar photovoltaic (PV), currently play an important role in the global technological scenario with the growing global demand for energy. Grid-connected or grid-tie PV power systems installed near the consumer are used to efficiently generate and distribute electricity without battery storage. Distributed generation brings several benefits such as lower transmission costs, fewer losses and reduction of urgent investments on huge power plants and transmission lines to supply the increasing electricity peak demand in many countries [1]. Distributed photovoltaic systems are rapidly growing and many studies show that PV and other renewable sources will highly contribute to the world's needs of electricity in next decades [2].

A grid-connected PV system comprises at least the following parts: solar module, inverter and utility grid. Fig. 1 illustrates a grid-connected PV system based on a two-stage grid-connected power converter.

This work was supported by FAPESP, processes numbers 10/15848-7 (Villalva, M. G.), 08/07956-4 (Ruppert, E.) and 10/50101-0 (Gazoli, J. R.); by Research Foundation of the State of Minas Gerais (FAPEMIG) and the Brazilian National Research Council (CNPq).

J. R. Gazoli (e-mail: gazoli@gmail.com) and E. Ruppert (e-mail: ruppert@fee.unicamp.br) are with the Department of Energy Control and Systems, University of Campinas, Campinas, SP, 13083-852, Brazil.

M. G. Villalva (e-mail: mvillalva@sorocaba.unesp.br) is with the Group of Automation and Integrated Systems, Universidade Estadual Paulista, Sorocaba, SP, 18087-180, Brazil.

T. G. Siqueira (e-mail: thaisgama@unifal-mg.edu.br) is with the Science and Technology Institute, Federal University of Alfenas, Poços de Caldas, 37715-400, Brazil.

The technical literature on power converters for grid-connected PV systems is extremely wide. Depending on the characteristics of the PV system (input and output voltage levels, rated power, electrical isolation) several converter topologies may be used. Along the past years many authors have proposed many different converters for PV applications. Some examples may be found in [3-5]. PV applications for residential use are rapidly growing towards the usage of module-integrated converters (MIC) generally in the power range bellow 500 W.

A literature review of MIC topologies was made in [6]. MIC converters may have a capacitor DC link or can employ a pseudo DC link with reduced capacitance or without capacitor. Fig. 1 shows a possible structure of a two-stage single-phase MIC inverter with a DC link capacitor. Many converter topologies may be employed and many kinds of MIC inverters can be found in the literature using half-bridge, full-bridge, push-pull, buck-boost, flyback, Cuk and other structures. This work uses a DC-AC H-bridge inverter with a high-frequency transformer and a low-frequency inverter cell in order to evaluate a resonant current control regulator to synthesize a sinusoidal output current. Alternatively, the DC-AC inverter with high-frequency transformer may be used with a transformerless DC-DC converter.

II. BRIEF REVIEW OF GRID-TIE POWER CONVERTERS BASED ON THE H-BRIDGE

Figure 2 shows a two-stage converter using an H-bridge inverter in the output [7] formed by switches Q3-Q6. The high-frequency transformer is employed on the DC side, which is composed by the half-bridge DC-DC converter formed by switches Q1-Q2 and the rectifiers D1-D4. One major characteristic of this structure is the fact that switches Q3-Q6 must support high voltages when the transformer turn ratio (N) is high. Thus, low-voltage MOSFETs may not be employed. This structure is generally employed in commercial PV converters [6].

Figure 3 shows an improvement on the converter of Fig. 2, where a full-bridge and a passive snubber are employed on the DC-DC side [8]. The output H-bridge inverter remains the same.

Figure 4 presents an H-bridge inverter employing a high-frequency output transformer, differently of the structures presented in Figs. 2 and 3. However, this converter operates as a voltage source and employs a bidirectional switch to allow working in the two half-cycles of the grid voltage. However, this converter presents low efficiency [9].

978-1-4673-2729-9/12/$31.00 ©2012 IEEE

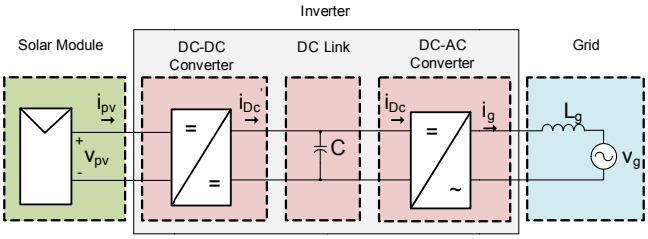

Fig. 1. General structure of a grid-connected PV system and internal structure of a single-phase inverter.

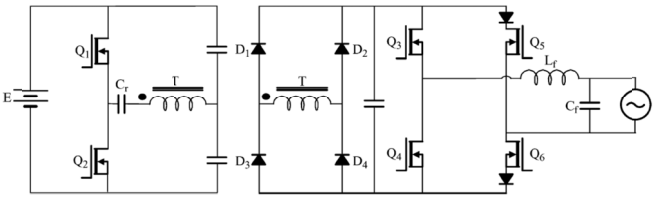

Fig. 2. Topology of a commercial PV converter using a high-frequency transformer on the DC-DC stage and an H-bridge inverter at the output [7].

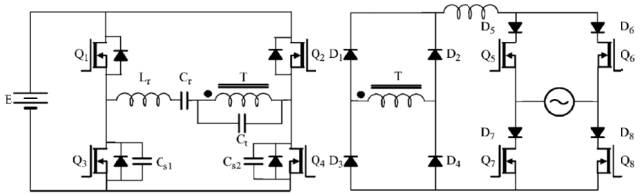

Fig. 3. An improved converter similar to the one presented in Fig. 2 where a full-bridge and a snubber are used in the DC-DC stage [8].

Figure 5 also presents a converter using an H-bridge with a high-frequency output transformer. However, in this converter a grid-frequency cycloconverter is employed. This type of structure is usually employed in applications in the range of several kilowatts and could theoretically be employed in MIC applications [10]. However, the high number of switches reduces the system efficiency.

Very few works in the literature present single-phase grid-connected H-bridges with high-frequency output transformer. This work uses the structure of Fig. 6 as an alternative to the structures presented in Figs. 3-5 and it represents a modification of the topology presented in Fig. 2.

This topology employs a high-frequency transformer on the DC side followed by a low-frequency inverter cell. This cell just commutates the output to define the current signal at every grid voltage semi-cycle.

The switches of the input bridge can be specified for low voltage with reduced series resistance, providing optimal efficiency for grid-connected PV applications. The presence of the step-up transformer avoids the necessity of a boost DC-DC stage, while keeping the system volume reduced in comparison with bulky systems based on grid-frequency transformers.

In Fig. 6, the input voltage E is applied to the input of the H-bridge voltage source inverter. The output voltage of the step-up 1:N transformer is modulated and the current flowing through inductor L is controlled in order to be sinusoidal. The

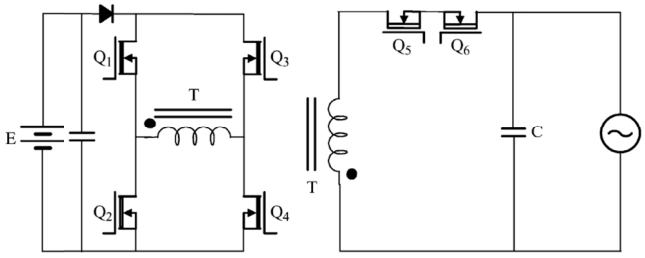

Fig. 4. A converter employing an H-bridge and a high-frequency output transformer connected to a bidirectional switch [9].

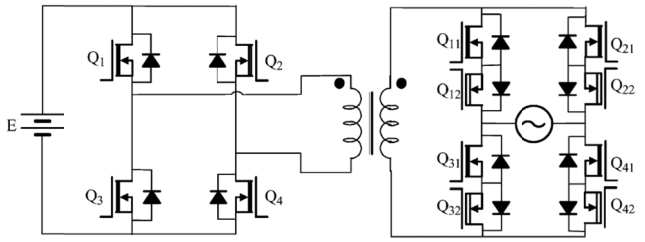

Fig. 5. Output HFT full-bridge topology with a cycloconverter [10].

output capacitive filter and the line inductance L_g help improving the harmonic filtering of the current injected into the grid. Because switches Q1-Q4 are subject to $E/2$, this structure may employ low-voltage power MOSFETs with small drain-source resistance. This structure may be used as a high-efficiency MIC, where the input voltage is generally lower than 70 V (typically twice the open-circuit voltage of commercial Si PV panels up to 60 cells).

III. SYSTEM MODEL

A. Principles

The inverter switches and the transformer are considered ideal for the purpose of system modeling. Furthermore, the H-bridge switching frequency is higher than the grid-frequency so that the switching ripple of the voltage and current at the output of the transformer may be neglected. Hence only the low-frequency behavior is analyzed and the average values within the switching periods are used in the small-signal modeling. The low-frequency inverter cell is considered a unitary gain for the purpose of small-signal analysis.

Switches Q1 and Q2 are complementary, as well as Q3 and Q4. There are three possible switching stages $U = (1, 0, -1)$. $U = 1$ corresponds to Q_1 and Q_4 closed; $U = -1$ corresponds to Q_3 and Q_2 closed; and $U = 0$ corresponds to all switches open. When the H-bridge is driven by a sinusoidal PWM with triangular carrier, only $U = 1$ and $U = -1$ are used [11] and one of the diagonals is always conducting.

The average voltage at the output of the transformer is given by (1), where d is the duty cycle of one H-bridge leg and $\bar{x}$ means the average value of the instantaneous variable $x(t)$ within one switching period.

The H-bridge inverter is connected to the grid through the output filter compose of L and C. With a closed-loop current controller, the circuit can behave as a controlled current

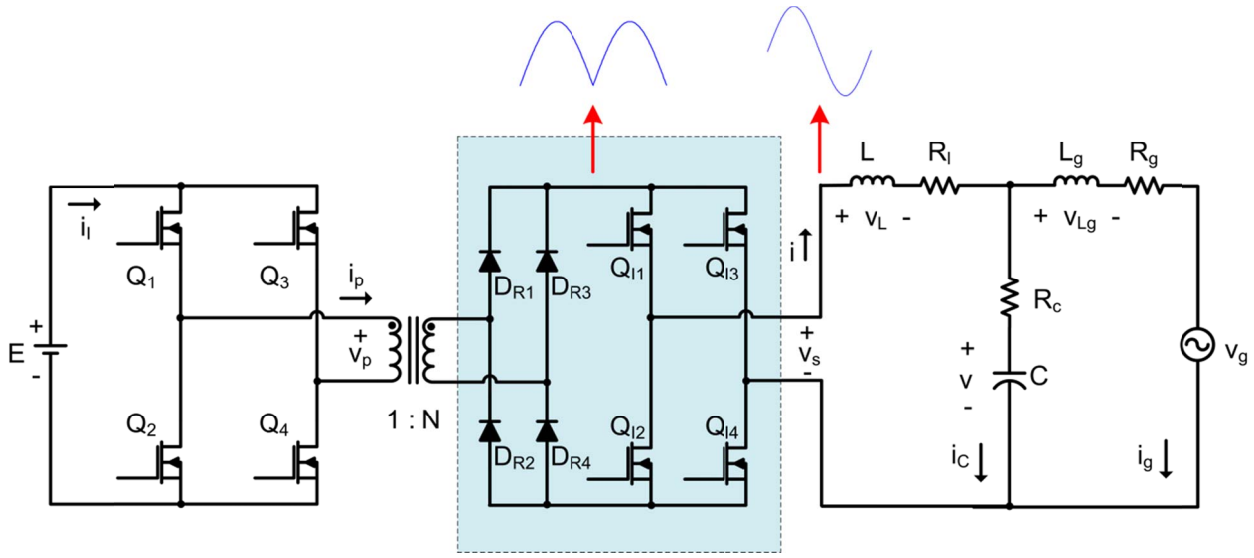

Fig. 6. Proposed single-phase grid-tie inverter with the H-bridge topology using a high-frequency transformer.

$$\bar{v}_s = NE\bar{U} = NE(2d - 1) \quad (1)$$

source connected to the grid. The high-frequency square voltage produced by the H-bridge is applied to the transformer, whose secondary applies a stepped-up square wave to the inductor. The voltage is then modulated in order to control the inductor current, which must be sinusoidal and synchronized with the grid voltage.

B. EMI filter design

The output RC filter composed of C and R_c is used to mitigate harmonic components of the output current, thus reducing the electromagnetic interference (EMI) of the grid-connected inverter.

The filter design is a critical issue in the inverter performance. The cut-off frequency of the filter is given by (2). This frequency must be higher than the current controller bandwidth so that the compensator design will not be influenced by the filter. On the other hand, the filter cut-off frequency must be lower than the switching frequency so that the high-frequency current harmonics can be correctly mitigated.

$$f_c = \frac{1}{2\pi R_c C} \quad (2)$$

Typically, the bandwidth of a power converter controller is chosen to be 1/10 of the switching frequency. Assuming the converter is switched at 20 kHz, the controller bandwidth will be 2 kHz and the filter cut-off frequency is arbitrarily chosen to be f_c= 3 kHz approximately. This filter can be built with C = 10 µF and R_c = 5 Ω.

C. Circuit parameters

The converter designed in this work has a nominal power of 200 W. The maximum input voltage is 40 V and the utility grid voltage is 127 Vrms at 60 Hz. In the simulations the grid line impedance is considered to be 0,2 + j0,037 Ω [12], which corresponds to L_g = 100 µH and R_g = 0,2 Ω. Table I presents the parameters used in the simulation and in the construction of the prototype inverter.

TABLE I
Inverter parameters.

Parameter	Description	Value
E	Input voltage	40 V
N	Transformer turns ratio	7
L	Inductor	4 mH
R_L	Series inductor resistance	0,2 Ω
C	Filter capacitor	10 µF
R_C	Filter resistor	5 Ω
L_G	Grid equivalent inductance	100 µH
R_G	Grid equivalent resistance	0,2 Ω
V_G	Grid voltage	127 V_{RMS}
P_o	Nominal output power	200 W
PF	Output power factor	1
f_S	Switching frequency	20 kHz

D. AC small-signals analysis

The small-signal analysis of the inverter and the output filter is necessary to obtain the inverter s-domain transfer function, which aids the design of the closed-loop current controller.

The system state variables of the circuit of Fig. 6 are i, $i_g$and v. The circuit state equations are (2)-(4).

$$NEU - R_l i - L\frac{di}{dt} = v + R_c C\frac{dv}{dt} \quad (2)$$

$$v_g + L_g\frac{di_g}{dt} + R_g i_g = v + R_c C\frac{dv}{dt} \quad (3)$$

$$C\frac{dv}{dt} = i - i_g \quad (4)$$

By using average variables and small signal components, the natural system behavior is preserved and the high frequency components are neglected. The substitution of small signal components as defined in (5) into the state equations leads to the small signal AC equations from which the system transfer function may be obtained. In (5), $\bar{x} = X + \hat{x}$, where X means the DC value of a variable and $\hat{x}$ means the small-signal AC perturbation.

$$\begin{aligned} \bar{\imath} &= I + \hat{\imath} \\ \bar{\imath}_g &= I_g + \hat{\imath}_g \\ \bar{v} &= V + \hat{v} \\ \bar{d} &= D + \hat{d} \end{aligned} \tag{5}$$

By replacing (5) in (2)-(3), applying the Laplace transformation to the resulting equations and neglecting the DC components, the small-signal AC linear equations given in (6) are found.

$$\begin{cases} (sL + R_l)\hat{\imath} = \hat{d}(2NE) - \hat{v}(sR_cC + 1) \\ \bar{\imath}_g(SL_g + R_g) = \hat{v}(sR_cC + 1) \\ \hat{\imath} = sC\hat{v} + \hat{\imath}_g \end{cases} \tag{6}$$

From equations (6) the s-domain transfer function (7) of the inverter output current is obtained.

$$G_{i_g d}(s) = \frac{\hat{\imath}_g}{\hat{d}} = 2NE\frac{sR_cC + 1}{a_3s^3 + a_2s^2 + a_1s + a_0} \tag{7}$$

where:

$$\begin{aligned} a_3 &= LL_gC \\ a_2 &= C\left[L\left(R_c + R_g\right) + L_g(R_L + R_c)\right] \\ a_1 &= R_LC\left(R_g + R_c\right) + R_gR_cC + L + L_g \\ a_0 &= R_g + R_L \end{aligned}$$

E. Model verification

In order to verify the validity of the transfer function of equation (7), an ACSWEEP analysis was done on the circuit of Fig. 6 in the PSIM simulator. The analysis was carried considering the behavior of the grid current $i_g$with small-signal variations of d. The analysis was done in the range of 10 Hz to 10 kHz and the result is plotted in Fig. 7 together with the Bode plot of the transfer function of equation (7).

IV. CONTROLLER SYSTEM

A. Controller structure

A current controller is used to produce a sinusoidal current synchronized with the grid voltage at the output of the RC filter (i.e. at the point of coupling of the inverter with the grid).

Figure 8 shows the block diagram of the current controller employed in this work, where i_{ref} is the current reference, $C(s)$ is the compensator, $G_{id}(s)$ is the inverter transfer function defined in (7), and H_i is the feedback gain.

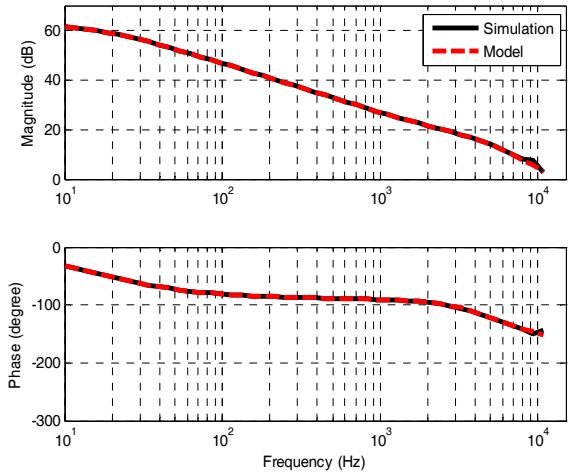

Fig. 7. Open-loop frequency responses of the simulated switched converter and of the small-signal model transfer function.

Many types of current controllers for grid-connected inverters have been proposed in the literature. Controllers employing linear PI (proportional and integral) or PID (proportional, integral and derivative) compensators are the most widely used due to their ease of implementation and effectiveness. A PI of PID compensator presents infinite gain at zero frequency, providing zero steady state error when the controlled variable has a steady state DC value [13,14]. When controlling sinusoidal currents, as is the case of the output current of the grid-tie inverter, PI-based controllers are not very effective and invariably present some amplitude or phase error even when the compensator is correctly tuned.

Furthermore, in practical applications PI or PID compensators are strongly affected by measurement DC errors and integrator very easily saturates. The infinite DC gain combined with the integrator action causes the integrator to saturate and the compensator response deteriorates. This problem can be minimized by eliminating measurement errors, however good results may not be always achieved in practice.

The proportional and resonant (P+RES) compensator is an alternative to the steady state error and integrator saturation of PI and PID compensators. Besides eliminating the problems discussed above, the P+RES compensator does not require coordinate transformations nor require PLL (phase-locked loop) synchronization, hence can be easily implemented in single-phase systems [13].

The P+RES compensator has the transfer function presented in (8), where k_p is the proportional gain, k_i is the integral gain, ω_0 is the synchronous angular frequency. The P+RES compensator has the same performance of a conventional PI combined with synchronous coordinate transformations [15]. Hence the current controller based on the P+RES compensator may achieve zero steady state error with sinusoidal currents.

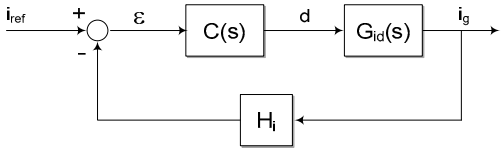

Fig. 8. Block diagram of the converter controller structure.

$$C(s) = k_p + \frac{2k_i s}{s^2 + \omega_0^2} \tag{8}$$

B. Controller discretization

The P+RES continuous-time transfer function of (8) can be implemented in microprocessor-based systems as the discrete compensator of (9), where $e(z)$ is the input signal (i.e. the control error) and $y(z)$ is the compensator output.

$$C_d(z) = \frac{y(z)}{e(z)} = \frac{b_0 + b_1 z^{-1} + b_2 z^{-2}}{a_0 + a_1 z^{-1} + a_2 z^{-2}} \tag{9}$$

The coefficients of (9) are obtained from the continuous transfer function by applying the bilinear or Tustin transformation of (10), where T_S is the sampling period.

$$C_d(z) = C(s)\big|_{s=\frac{2}{T_S}\frac{z-1}{z+1}} \tag{10}$$

By applying (10) to (9) the coefficients of the P+RES compensator are:

$$\begin{gathered} a_0 = 1 \\ a_1 = 2 - 16/(T_s^2\omega_0^2 + 4) \\ a_2 = 1 \\ b_0 = k_p + 4T_s k_i/(T_s^2\omega_0^2 + 4) \\ b_1 = 2k_p - 16k_p/(T_s^2\omega_0^2 + 4) \\ b_2 = k_p - 4T_s k_i/(T_s^2\omega_0^2 + 4) \end{gathered} \tag{11}$$

Equation (9) may be written as the difference equation (12), which corresponds to a direct transposed IIR (infinite impulse response) filter.

$$\begin{aligned} y[k] = b_0 e[k] + b_1 e[k-1] + b_2 e[k-2] \\ - a_1 y[k-1] - a_2 y[k-2] \end{aligned} \tag{12}$$

C. Compensator design

The equivalence between the frequency responses of the PI and P+RES compensators above the cross-over frequency permits to design k_p by adjusting the gain in order to achieve the desired bandwidth and phase margin. Typically, the cross-over frequency is 1/10 of the inverter switching frequency and the phase margin must be chosen in order to warranty system stability. Generally the value of k_i used in the P+RES compensator may be the same as used in the PI. As a rule of thumb, one can use in the P+RES compensator the same values of k_p and k_i that would be used in the design of a conventional PI compensator.

As an example, one first defines k_p = 0.01 and k_i = 10^4 and the compensator transfer function is given by (13).

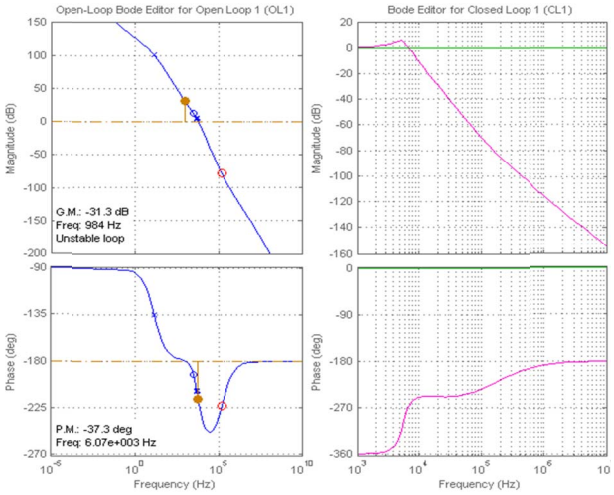

Fig. 9. Open and closed-loop frequency responses of the system with $C_{PI}(s)$ – unstable system.

Figure 9 shows the Bode plots of the open and closed-loop system. It is evident that the system is unstable. The graphs were obtained with the RLTOOL in MATLAB.

$$C_{PI}(s) = \frac{0.01s + 10^4}{s} \tag{13}$$

In next step the proportional gain and the compensator zero are adjusted so that the cross-over frequency is set to 2 kHz and a phase margin of 46.8º is achieved, as shown in Fig. 10. The system is now stable with k_p = 0.06623 and k_i = 657.1.

The last step is to use the determined gains in the P+RES compensator whose transfer function is given by (14). Fig. 11 shows the frequency responses of the system employing the P+RES compensator.

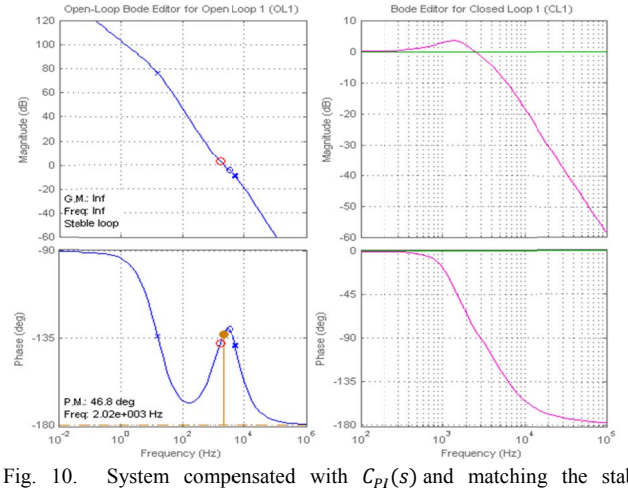

Fig. 10. System compensated with $C_{PI}(s)$ and matching the stability requirements.

The correct placement of the cut-off frequency of the EMI filter at the output of the inverter strongly affects the design of the control loop. The filter modifies the phase of the system and introduces a resonance that makes difficult the compensator design if the cut-off frequency is too close to the closed-loop cross-over frequency. The filter cut-off frequency

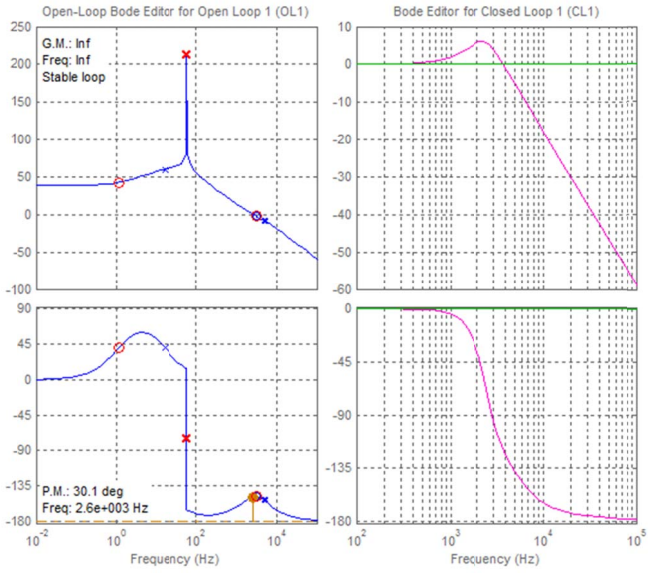

Fig. 11. System compensated with $C_{P+RES}(s)$ and matching the stability requirements.

$$C_{P+RES}(s) = \frac{0.06623s^2 + 1314s + 9413}{s^2 + 1.421e5} \qquad (14)$$

must be set above the cross-over frequency and a resistance in series with the filter capacitance must be used in order to introduce some dumping, which makes easier the compensator design and reduces the effect of the filter resonance. By introducing this resistance the margin phase of the compensated system is increased.

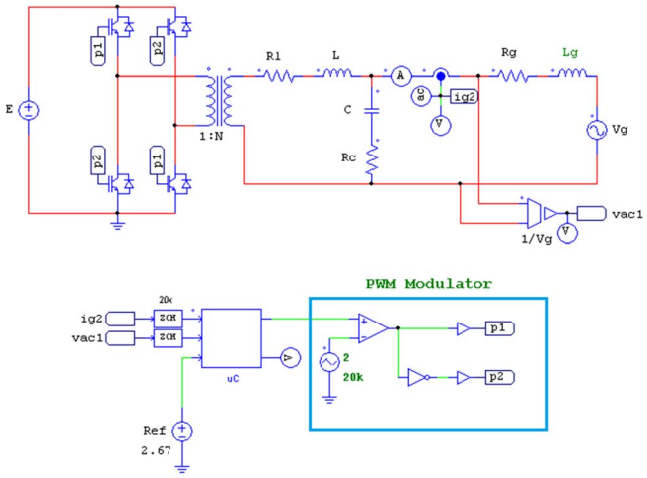

Fig. 12. Simulation diagram using PSIM.

V. SIMULATIONS

A simulation was carried using the software PSIM. The simulated circuit is shown in Fig. 12 and the simulation result is presented in Fig. 13. The inverter output current tracks the sinusoidal reference and takes less than a quarter of the 60 Hz cycle in order to achieve steady state. At t = 0.037 s a

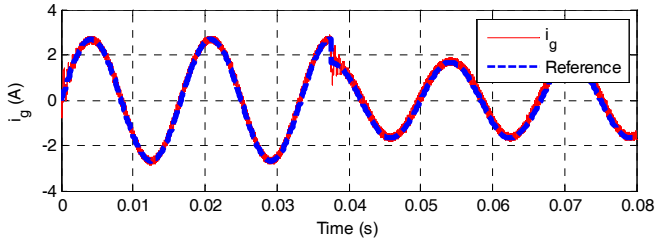

Fig. 13. Output current simulation response with a 40% reference step decrease at time 0.037 s.

disturbance is introduced in the system and the current rapidly tracks the new reference.

VI. PROTOTYPE

A 200 W prototype was developed in the laboratory in order to evaluate the control performance. Figure 14 shows the micro-inverter and its auxiliary circuitry. The digital control was implemented with the TMS320F28335 digital signal controller (DSP) and the high-frequency transformer was built using a RM14 core with 3C90 material, from Ferroxcube.

The experimental results are shown in Figs. 15 and 16. Fig. 15 shows the output current in phase with the grid voltage. The exact sync between the output current and the grid voltage is a result of the P+RES compensator. The input current of the micro-inverter, also shown in Fig. 15, has twice the line frequency.

Figure 16 shows the output current and the internal reference current of the digital controller measured with a digital to analog converter. One can notice that the proposed P+RES controller effectively achieves zero steady-state error.

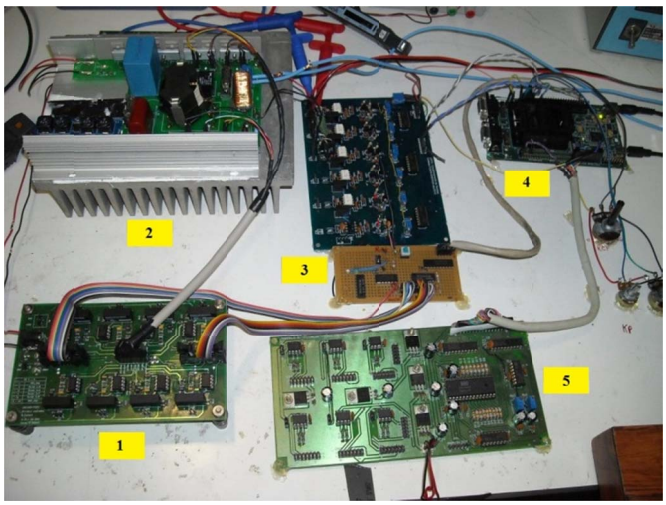

Fig. 14. 200 W experimental micro-inverter prototype (2) and auxiliary boards: drivers (1); sensing (3); micro-controller (4) and digital-to-analog converter (5).

VII. CONCLUSION

This work has analyzed a single-phase grid-tie inverter based on the H-bridge topology and using a high-frequency transformer. The subjects of small-signal analysis, modeling,

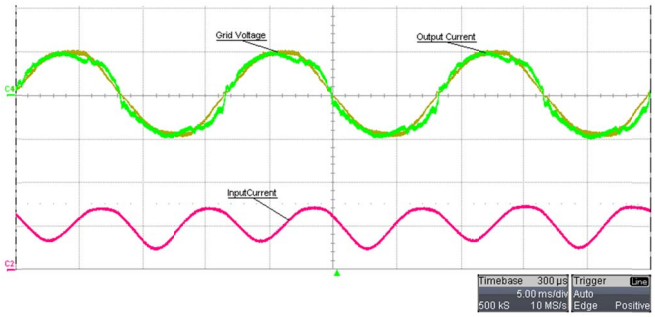

Fig. 15. Grid voltage (200V/div), output current (2A/div) and input current (5A/div) of the 200 W experimental prototype (Horizontal: 5 ms/div).

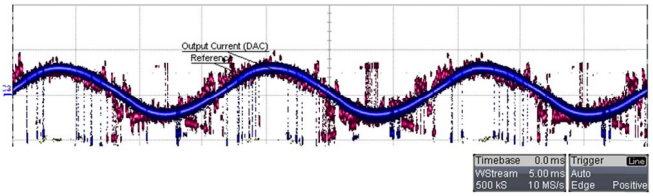

Fig. 16. Output current (2 A/div) and its reference (2 A/div) (Horizontal: 5 ms/div).

control design and simulation have been explored in the paper. The design of a P+RES compensator has been studied and the advantages of this kind of compensator are the simplicity for implementation in single-phase systems and zero steady state error with sinusoidal current.

One major advantage of the system presented in this paper is the possibility of using low-voltage power switches, such as low-resistance MOSFETs, differently of other types of single-phase inverters presented in the literature. The usage of a high-frequency transformer allows better efficiency in comparison with grid-frequency transformers generally employed.

A 200 W electronic prototype developed in the laboratory was presented. The results show that the resonant controller achieves zero steady-state error, what means a unit power factor at the micro-inverter output.

VIII. REFERENCES

[1] European Photovoltaic Industry Association, Greenpace. *Solar Generation 6 – Executive Summary*. [Online]. Available: http://www.epia.org/fileadmin/EPIA_docs/documents/Solar_Generation_6_Executive_Summary2.pdf

[2] European *Renewable Energy Council. Renewable Energy Scenario to 2040*. [Online]. Available: http://www.erec.org/fileadmin/erec_docs/Documents/Publications/EREC_Scenario_2040.pdf

[3] Kjaer, S. B., Pedersen, J. and Blaabjerg, "Power inverter topologies for photovoltaic modules-a review", *in Proc. 37th IAS Ind. Applications Conf.*, v. 2, pp. 782–788, 2002.

[4] Blaabjerg, F. "Power converters and control of renewable energy systems", *in Proc. 37th IEEE PESC*, 2006.

[5] Kjaer, S. B., Pedersen, J. and Blaabjerg, F. "A review of single-phase grid-connected inverters for photovoltaic modules", *in IEEE Transactions on Industry Applications*, v. 41, pp. 1292-1306, 2005.

[6] Quan Li and Wolfs, P. "A review of the single phase photovoltaic module integrated converter topologies with three different dc link configurations", *in IEEE Transactions on Power Electronics*, v. 23, pp. 1320, 2008.

[7] Lohner, A., Meyer, T and Nagel, A. "A new panel-integratable inverter concept for grid-connected photovoltaic systems," *in Proc. IEEE ISIE*, pp. 827–831, 1996.

[8] Prapanavarat, C., Barnes, M. and Jenkins, N. "Investigation of the performance of a photovoltaic AC module" *in IEE Proceeding of Generation, Transmission and Distribution*, vol. 149, no. 4, pp. 472–478, 2000.

[9] Fernandez, A., Sebastian, J., Hernando, M. M., Arias, M. and Perez, G. "Single stage inverter for a direct ac connection of a photovoltaic cell module" in Proc. IEEE PESC, pp. 93–98, 2006.

[10] Beristain, J., Bordonau, J., Gilabert, A. and Velasco, G. "Synthesis and modulation of a single phase dc/ac converter with high-frequency isolation in photovoltaic energy applications" *in Proc. IEEE PESC*, pp. 1191–1196, 2003.

[11] Boudjema, F., Boscardin, M., Bidan, P., Marpinard, J. C., Valentin, M. and Abatut, J. L. "Vss approach to a full bridge buck converter used for AC sine voltage generation" *in 15th Annual Conference of IEEE Industrial Electronics Society*, IECON, vol. 1, pp. 82–88, 1989.

[12] Wang, X. and Freitas, W., "Impact of positive-feedback anti-islanding methods on small-signal stability of inverter-based distributed generation", *in IEEE Trans. on Energy Conversion*, vol. 23, pp. 923-931, 2008.

[13] Villalva, M. G., "Conversor eletrônico de potência trifásico para sistema fotovoltaico conectado à rede elétrica", PhD thesis, *Univ. of Campinas, Brazil*, 2010.

[14] Gazoli, J. R., "Microinversor monofásico para sistema solar fotovoltaico conectado à rede elétrica". Msc thesis, Univ. of Campinas, Brazil, 2011.

[15] Zmood, D., Holmes, D.N., "Stationary frame current regulation of PWM inverters with zero steady-state error," *in IEEE Transactions on Power Electronics*, vol. 18, pp. 814–822, 2003.

IX. BIOGRAPHIES

Jonas Rafael Gazoli was born in Americana, São Paulo, Brazil, in 1983. He received the B.Sc. and M.Sc. degrees in electrical engineering in 2008 and 2010, respectively, from the University of Campinas (UNICAMP), Brazil, where he is currently working toward the Ph.D. degree.

He was with the Power Electronics Group, University of Padova, Italy, in 2008-2009, where he worked with high voltage gain non-isolated power converters for photovoltaic systems.

His current research interests include power electronics for solar energy conversion and control strategies for electrical drives.

Marcelo Gradella Villalva was born in Campinas, Sao Paulo, Brazil, in 1978. He received the B.Sc., M.Sc. and Ph.D. degrees in electrical engineering in 2002, 2005 and 2010, respectively, from the University of Campinas (UNICAMP), Brazil, where he is currently developing his postdoctoral research.

Since 2011, he has been with the UNESP as a Full Professor and Researcher.

His current research interests include active filters, modeling and control of electronic converters, photovoltaic energy systems, distributed generation, and artificial intelligence applied to power electronics.

Thais G. Siqueira was born in 1978, in the city of Belém, Brazil. She received a BS degree in Applied Mathematics from UNICAMP, Brazil, in 2000 and obtained her M.Sc. and Ph.D. degrees in Electrical and Computer Engineering School of UNICAMP, Brazil, in 2003 and 2009, respectively.

She was a Ph.D. visiting student at Cornell University in 2006. She is currently Professor at Institute of Science and Technology, UNIFAL, Poços de Caldas, Brazil with research interests involving the planning and operation of electrical power system.

Ernesto Ruppert Filho was born in Jundiaí, São Paulo, Brazil. He received the B.Sc., M.Sc., and Ph.D. degrees in electrical engineering from the University of Campinas (UNICAMP), Campinas, Brazil, in 1971, 1974, and 1982, respectively.

He was engaged as a project engineer and/or consultant, in Brazil and abroad, for several large companies such as Itaipu, Petrobras, General Electric, Alstom, Copel, CPFL, and Elektro. Since 1972, he has been with the UNICAMP as a Professor and Researcher. He is currently a Full Professor and coordinates several research projects with private companies and public institutions in Brazil.

His current research interests include power electronics, superconductor current limiters, electrical power systems, distributed generation, electric machines, and motor drives. He has authored or coauthored many technical papers published in international journals and conferences